American Industrial Hygiene Association Journal

ISSN: 0002-8894 (Print) (Online) Journal homepage: https://www.tandfonline.com/loi/aiha20

Imaging Indoor Tracer-Gas Concentrations with Computed Tomography: Experimental Results with a Remote Sensing FTIR System

M.G. Yost , A.J. Gadgil , A.C. Drescher , Y. Zhou , M.A. Simonds , S.P. Levine , W.W. Nazaroff & P.A. Saisan

To cite this article: M.G. Yost , A.J. Gadgil , A.C. Drescher , Y. Zhou , M.A. Simonds , S.P. Levine , W.W. Nazaroff & P.A. Saisan (1994) Imaging Indoor Tracer-Gas Concentrations with Computed Tomography: Experimental Results with a Remote Sensing FTIR System, American Industrial Hygiene Association Journal, 55:5, 395-402, DOI: 10.1080/15428119491018835

To link to this article: https://doi.org/10.1080/15428119491018835

AIHA JOURNAL Advances in Industrial & Environmental Hygiene

AM. IND. HYG. ASSOC. J. 55(5):00–00 (1994)

Imaging Indoor Tracer-Gas Concentrations with Computed Tomography: Experimental Results with a Remote Sensing FTIR System

M.G. Yost[a]
A.J. Gadgil[b]
A.C. Drescher[b]
Y. Zhou[c]
M.A. Simonds[d]
S.P. Levine[d]
W.W. Nazaroff[e]
P.A. Saisan[b]

[a]Department of Environmental Health, SC-34, School of Public Health and Community Medicine, University of Washington, Seattle, WA 98195; [b]Indoor Environment Program, Energy and Environment Division, Lawrence Berkeley Laboratory, Berkeley, CA 94720; [c]School of Public Health, University of California, Berkeley, CA 94720; [d]School of Public Health, University of Michigan, Ann Arbor, MI 98109; [e]Department of Civil Engineering, University of California, Berkeley, CA 94720

This work demonstrates for the first time the feasibility of computed tomography (CT) reconstructions of pollutant concentrations in a real room setting. A remote sensing Fourier transform infrared spectrometer was mounted on a moving base in a controlled ventilation chamber. A passive tracer was released from a point source into the room under constant ventilation conditions. A series of experiments gathered multiple path-averaged measurements in a two-dimensional plane for CT reconstruction. Simultaneous readings were gathered with a multiple-point sampling array for later comparison to the CT reconstructed concentrations. Good qualitative agreement between the reconstruction and point sample data was obtained. Limitations encountered due to the temporal resolution, size, and geometry of the experimental apparatus are clearly surmountable with better instrumentation.

The assumption that indoor air mixes instantly lies at the foundation of indoor air quality research and practice. Standards for building ventilation, research on indoor pollutant concentrations, and the assessment of human exposures and associated health risks all are based on this crude assumption. However, because of the experimental and theoretical challenges encountered in studying mixing in indoor environments, this assumption has not received attention commensurate with its importance.

Numerical models for simulating forced and natural convection flow in rooms have been developed recently. These have been applied to heat and pollutant transport in rooms.[1] But owing to the complexity of the models, the simulations use substantial simplifications of the boundary conditions that define the flow. Only a few techniques exist, such as

Partial financial support for this research was provided by the National Institute of Occupational Safety and Health, grant RO1-OH-02666; National Science Foundation, grant BCS-9057298; Cigarette and Tobacco Surtax Fund, State of California, through the Tobacco-Related Disease Research Program, University of California, grant RT 666; and Assistant Secretary for Conservation and Renewable Energy, Office of Building Technologies, Building Systems and Materials Division of the U.S. Department of Energy, contract DE-AC03-76SF00098.

sonic[2] and hot wire anemometry, for obtaining detailed measurements of indoor air flows, and the available experimental data are so sparse that even the simulations undertaken with over-simplified boundary conditions cannot be adequately validated.[3]

Indoor air mixing and ventilation efficiency are commonly studied experimentally using tracer gas techniques.[4,5] These studies have employed either multiple arrays of pump-and-tube samplers, or a small array of sampling tubes that is moved to various locations in the space under investigation. Air samples are collected, then analyzed, to measure the tracer gas concentrations and thus infer the motion of air and the dispersion of pollutants. The temporal and spatial resolution that may be achieved by this approach is severely limited. There is no rapid and minimally intrusive experimental technique for determining room pollutant concentrations over large areas (and thus evaluating ventilation efficiency, pollutant transport, and mixing).

Steady advances in infrared detection and quantitative analysis of infrared spectra for airborne pollutants have led to the development of a new class of direct-reading instruments, based on the remote sensing Fourier transform infrared (RS-FTIR) spectrometer. These instruments use an infrared beam to probe the air and are capable of detecting a wide variety of contaminant species in situ at concentrations as low as a few parts per million over path lengths of many meters.[6] Such instruments recently have been scaled down to transportable size and are being used for concentration measurements of airborne gases in workplaces and outdoors.[7]

A fundamental feature of RS-FTIR instruments is that they provide an integrated measurement of the contaminant mass in the beam path. This normally is converted to a path average molar concentration by dividing the measurement (e.g., ppm-meters) by the known path length. A consequence of this spatial averaging is that some quantities of interest, such as the peak concentration along the beam path, cannot be obtained without additional information on the spatial distribution of contaminants in the beam.

The aim of the research described here was to demonstrate by experiment a new method to quantify pollutant transport using a potentially rapid and minimally intrusive sensing technique: RS-FTIR detection of a tracer gas coupled with computed tomography (CT). CT provides a set of numerical techniques for reconstructing the spatial concentration distribution from a set of path-integrated sample projections through the space. Typically this involves transforming a set of multiple beam path measurements passing through a plane at many angles into a two-dimensional grid of pixel values corresponding to local concentrations. CT data processing techniques enhance our interpretation of raw path integrated measurements by providing the ability to resolve local concentrations.

This exploratory research demonstrates through a proof-of-concept experiment that CT can provide a tool to investigate pollutant dispersion indoors. Further development of this tool could lead to significant advances in indoor atmospheric science by facilitating research on the many factors that influence indoor air mixing. This approach also has applications to situations involving source location and identification.

Quantitative application of near-visible optical tomography for gas flows was first reported in 1986.[8] Experimental studies have thus far been limited to imaging small areas (on the order of a few square centimeters).[9–11] In the published literature, optical CT using a laser as a source has been suggested for assessing outdoor airborne pollutants in urban air basins.[12,13] More recently, CT reconstruction of simulated indoor gas concentrations was demonstrated assuming idealized sources and detectors surrounding the perimeter of a plane cross-section of an industrial workplace.[14–16]

MATERIALS AND METHODS

An RS-FTIR spectrometer system was mounted on a moving base in a controlled ventilation chamber. A tracer was released continuously from a point source into the room under constant ventilation conditions. A series of experiments gathered multiple path-averaged measurements in a two-dimensional plane for CT reconstruction. The measurement plane was midway between the floor and ceiling of the room, 1.37 m (4.5 ft) above and parallel to the floor. Simultaneous readings were gathered with a multiple point sampling array in the same plane for later comparison to the CT reconstructed concentrations.

Test Chamber

The test chamber illustrated in Figure 1a was designed to provide ventilation in a horizontal plug-flow arrangement. The chamber is described in detail elsewhere so only a brief description follows.[17] The 143 m^3 (5050 ft^3) working section has two plenums covering opposing side walls to distribute the supply and exhaust air. Other room walls are sealed to reduce leakage. Two industrial blowers provide push-pull mechanical ventilation and have speed regulation of 1% around the set point. The fans were set for a volume flow rate through the chamber of about 142 m^3/min (5000 ft^3), giving a residence time for air in the room of 1 minute (60 air changes per hour) and a mean velocity of approximately 10 cm/sec (20 ft/min).

The chamber is equipped with a custom-designed, computer controlled sampling system that sequentially monitors air concentrations at 14 points. Each sample point is connected by polyethylene tubing to a 3-way solenoid valve and exhaust manifold. Air samples are drawn continuously at a rate of 5 cc/sec from each sample line into the exhaust manifold to minimize the delay in response time due to the dead volume in the tubing. The samples pass into a flame ionization detector (FID, Century Instruments, Arkansas City, Kan.), which provides a 1.0 mV/ppm analog output signal that is sampled and stored in a computer. The FID has a range of 0.2 to 2000 ppm with a response time (0 to 90% of full scale) of about 4 seconds.

Acetone vapor was the tracer gas used in this study. The vapor was generated by passing 1 L/min dry nitrogen

through liquid acetone in a 250 mL glass bubbler kept in a water bath set at 35 °C. Temperature regulation of the water bath over time was better than 0.1 °C. The bubbler output was connected to a 4 L glass mixing chamber and then passed through polyethylene tubing to a 2-cm diameter porous-ceramic spherical diffuser, effectively creating a point source. A needle valve controlled the flow of nitrogen gas; the flow rate was measured by a rotameter calibrated with nitrogen. The source was positioned 60 cm (2 ft) upstream of the geometric center of the room along the inlet-to-outlet center line axis, 3 cm (1.2 in) above the measurement plane (see Figures 1a and 1b). An FID sample port in the exhaust air duct monitored the generation rate of the source, which was constant during these experiments.

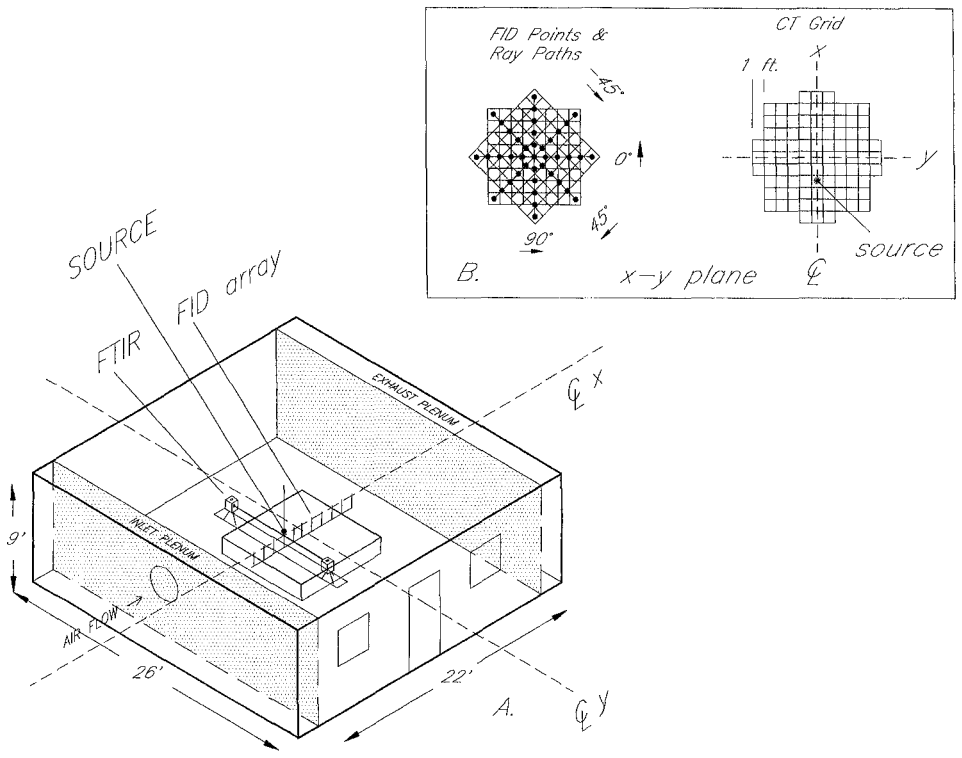

FIGURE 1. (a) Isometric view of the test facility, showing the RS-FTIR mounted on the translating table attached to the rotating base. The FID array was arranged perpendicular to the beam path and rotated with the base. The source was suspended from the ceiling at a fixed location 60 cm (2 ft) upstream from the geometric center of the room. (b) Plan view of the ray path geometry and CT grid used for the reconstructions. Dark dots mark locations corresponding to FID array sampling points for each projection angle. Arrows indicate the direction of movement for the translating stage when scanning one of the four projection angles (0°, 90°, ± 45°) defined by the position of the rotating base.

RS-FTIR Description

FTIR data were collected using a Nicolet ST-1 FTIR spectrometer equipped with a liquid-nitrogen cooled mercury-cadmium-telluride detector (Nicolet Inst. Corp., Madison, Wis.). The optical bench was modified by Nicolet for remote optical sensing as described elsewhere.[18] The IR source (1300 °K filament) and swinging mirror interferometer (2 cm^{-1} resolution) were mounted together in a cabinet on a tripod, from which emerged a 5-cm diameter IR beam with a coaxial 1.5 mW visible laser beam to assist with aiming. The separate tripod-mounted detector was fitted to a 20-cm diameter Cassagrain telescope, which collected the IR beam. Sample scanning, data collection, and spectral analysis were performed using an IBM-compatible 386 personal computer.

The RS-FTIR was mounted on a specially constructed translating table attached to a floor-mounted rotational platform on a central pivot (Figure 1a). The source-interferometer and detector were arranged in a straight line 3-m beam path on the translating stage. A remotely controlled traversing system powered by DC motors positioned the translating table (and beam path) at 30 cm (1 ft) fixed intervals in order to gather a set of parallel ray paths forming one projection; the platform was then rotated to a new position and the traverse repeated to gather a projection at another angle.

The multipoint FID sample array was positioned along a midline of the rotating platform. Eleven sample points were arranged at 30 cm (1 ft) intervals along a line perpendicular to the beam path and translating stage. The sample points were scanned continuously by the computer sampling network. Three additional ports monitored the inlet air, exhaust air, and a 125 ppm span gas standard. These additional samples furnished a check on the room background, source emission rate, and the detector calibration. Each port was sampled for 10 seconds, followed by a 10 second delay between samples to preclude any switching artifacts.

Each experimental run consisted of data gathered for four angular projections (90°, 45°, 0°, and –45°). Each projection angle resulted in a corresponding fixed position for the FID array aligned perpendicular to the beam path. The entire FID array was scanned every 5 minutes and 9 complete array scans were stored in a 45-minute sampling period for a single projection angle. The individual 10-second readings from the FID sample points were averaged together over the 45-minute period for each projection angle, and four of these 45-minute projections constituted an experimental run spanning 180 minutes. Simultaneously with the FID data collection, the RS-FTIR was positioned at one of the 9 ray path locations along the projection and averaged over a 5-minute interval to ensure steady-state conditions.

At the completion of each projection scan, the platform rotated to a new angle and a new set of ray scans was gathered.

Calibration

The FID was calibrated over a range of 1 to 1500 ppm using commercially available gas cylinders (Matheson Gas Products). Two factory analyzed primary gas standards, 100 ppm and 1500 ppm (± 1%) acetone in air were diluted immediately prior to calibration in hydrocarbon-free air to create working standards. Dilutions were prepared by measuring a volume of this air into 20 L Tedlar bags with a calibrated dry test meter, and then injecting a volume of the primary gas into the bags with a gastight syringe to obtain intermediate concentrations of 5, 10, 50, 500, and 1000 ppm.

Quantitative analysis of IR spectra were performed with a least-squares fit program and a spectral library covering the range of 4000 to 600 cm^{-1} at 2.0 cm^{-1} resolution. Least squares quantification used a 53 ppm acetone plus water and CO_2 reference spectra, in two analysis windows at 2800–3200 cm^{-1} and 1150–1260 cm^{-1}. The spectral library was obtained from tests with a 10-m gas cell. The choice of this library and the use of the least squares algorithm for analysis are described elsewhere.[19]

Computational Methods

The FID point data were interpolated using SURFER (Golden Software, Golden, Colo.) to produce a two-dimensional uniform grid of concentration values. A kriging algorithm was used to find minimum variance estimates of these grid values. Kriging is a geostatistical technique for estimating a grid of values from a set of arbitrarily positioned point measurements that uses the spatial correlation between points to find minimum variance estimates of intermediate grid points.[20]

Computed tomography comprises a variety of different numerical methods for reconstructing images from projections.[21] The term "image" is used here in the broadest sense, referring to a spatial distribution of a measurable physical property, such as density or temperature,[22] in a two-dimensional slice of matter. The relative performance of different CT methods depends on the type of reconstruction algorithm being used, the characteristics of the distributions being reconstructed, the sampling density, and the noisiness of the projection data.

Briefly, the reconstruction was achieved as follows: an initial guess of the concentration distribution was improved on in successive iterations by comparing computed ray averages resulting from the estimated distribution with the measured ray averages. A dimensionless relaxation parameter was used to regulate the speed of convergence and ensure stability against numerical oscillations. The only constraint placed on the reconstruction was that pixel concentrations could not be less than zero. Thus, after every iteration pixels whose concentrations were negative were assigned a value of zero.

There are two major parts in an iterative CT algorithm: (1) a formula to calculate corrections to the current estimates

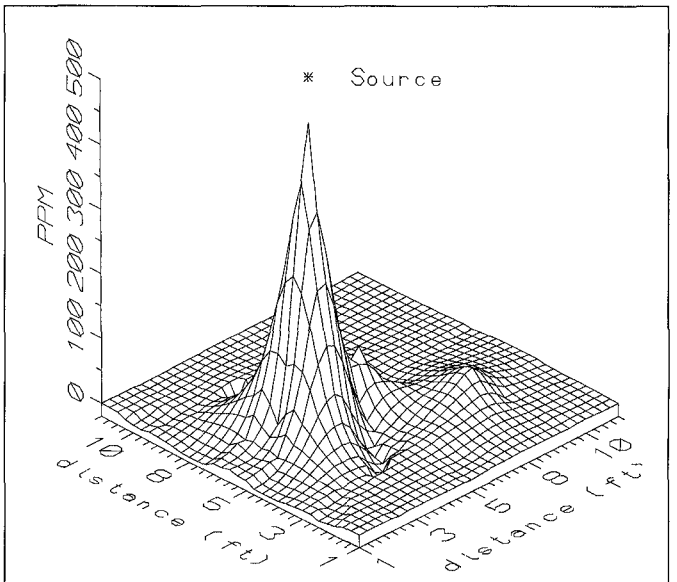

FIGURE 2. Acetone concentrations obtained from kriging the FID data

of pixel concentrations based on the discrepancy between computed and measured ray average concentrations; and (2) a method for updating the computed pixel and ray average concentrations. The authors updated all the pixels sequentially, as done in ILST algorithms.[23] The formula used to calculate new pixel concentrations was:

$$C_{p,\,i+1} = C_{p,\,i} + \frac{\gamma}{N_p} \sum_{r=1}^{r=N_p} \left(RAM_r - RAC_{r,\,i}\right) \frac{\ell_{r,p}}{L_r}$$

where

$C_{p,\,i+1}$ = the concentration in pixel p at the i th iteration
γ = relaxation parameter
N_p = number of rays passing through the pixel p
RAM_r = measured path-average concentration of ray r
$RAC_{r,\,i}$ = calculated path-average concentration of ray r at the i^{th} iteration
$\ell_{r,\,p}$ = the segment length of ray r passing through pixel p
L_r = the total length of ray r.

Based on the work of Peterson[24] (where the equivalent formula is referred to as ART1) and tests of this and several similar formulas applied to real and synthetic data,[25] the above formula was expected to produce reasonable reconstructions while being robust to input noise.

Estimates of pixel concentrations were updated according to ILST. New ray average concentrations were calculated only after all pixels had been updated. The CT program written specifically for the geometry of this experiment was thus based on both the ART1 formula for calculating the corrections and on the ILST correction scheme for updating the pixel estimates. The computer program was first tested on synthetic Gaussian distributions and on simulated profiles having steep concentration gradients similar to those expected in the real data. Good results were achieved even when

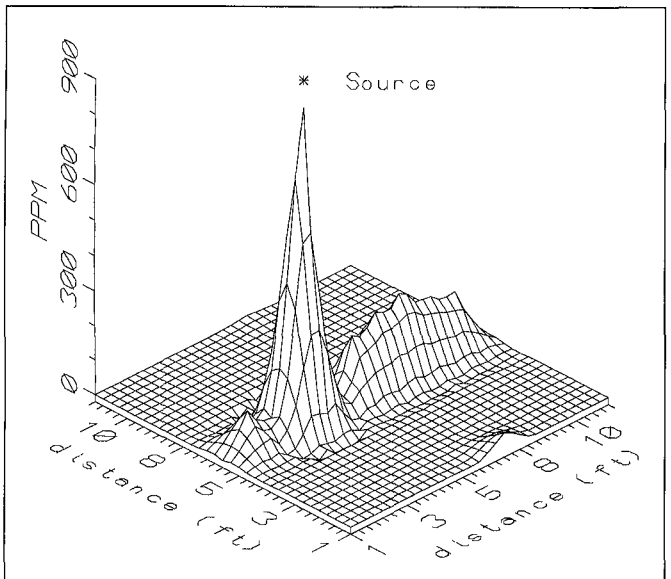

FIGURE 3. Acetone concentrations reconstructed from ray path averages from RS-FTIR data. ILST algorithm used for CT reconstruction, 1000 iterations, relaxation parameter = 6, sigma at convergence = 0.4.

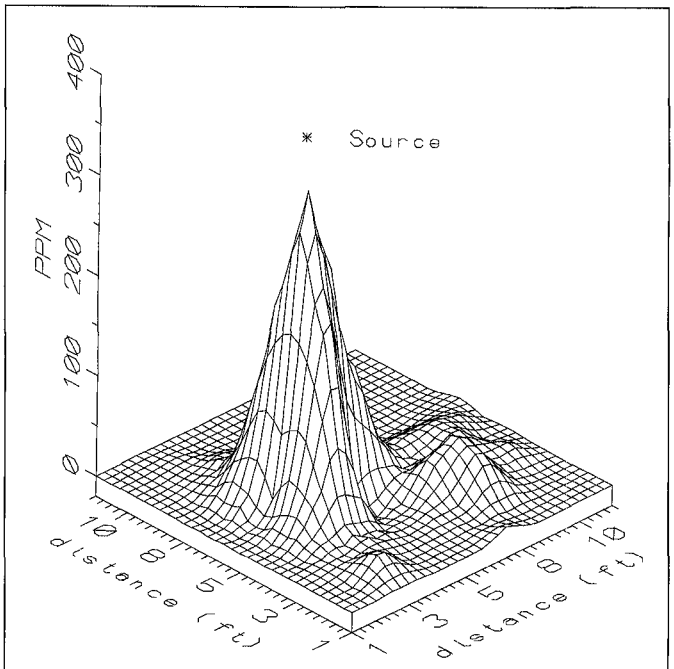

FIGURE 4. Acetone concentrations reconstructed from ray path averages calculated from the kriged FID data (Figure 2). ILST algorithm used for CT reconstruction, 1000 iterations, relaxation parameter = 10, sigma at convergence = 0.0024.

randomly generated noise with a coefficient of variation between 10% and 50% was added to the synthetic ray average concentration data.

The area covered by rays was divided into square pixels with a width equal to the distance between parallel rays (0.3 m, 1 ft). This resulted in 93 pixels (9 by 9, plus 3 pixels along the middle section of each edge), each having between 2 and 6 of the 36 rays passing through it (Figure 1b). A parameter, sigma, was defined to quantify the overall extent of agreement between the average concentration along a specific ray path of the reconstructed image (RAC = ray average calculated) and that measured for the physical system (RAM = ray average measured):

$$\sigma = \sqrt{\frac{\sum_{\text{all rays}} (\text{RAM} - \text{RAC})^2}{\sum_{\text{all rays}} (\text{RAM})^2}}$$

A reconstructed distribution with a lower value of sigma has a better overall agreement between the average concentrations along the rays and measured data. However, a low sigma value does not guarantee a close match between pixel-by-pixel reconstructed concentrations and those in the measured physical system (see Discussion).

RESULTS

The experiments produced two data sets, one consisting of 36 beam-path-averaged values (9 ray paths for each of 4 projection angles) and the second consisting of 44 point values from the FID array (Figure 1b). The rays were time averaged over 5-minute intervals while the point values were time averaged over 45-minute intervals (typical SD of FID values ~ 100%). Figure 2 shows a surface plot of the kriged FID grid values representing the plume as captured by the FID array.

Applying the tomographic reconstruction to the FTIR ray average data resulted in the concentration distribution shown in Figure 3. The main features of the acetone plume (the source and the direction of advection) are clearly recognizable, including the region of slightly increasing concentration downwind of the source that was apparent in the kriged data. However, the relatively high value of sigma, 0.4, which was the best achievable value over a wide range of relaxation parameters and number of iterations, indicates that the reconstructed concentration distribution was based on an internally inconsistent (or noisy) set of ray average values (see Discussion).

To test the ability of the CT program to reconstruct a concentration profile where the concentration values are known, the kriged FID data of Figure 2 were used to calculate ray averages and produce a synthetic data set of concentrations corresponding to the 93 pixels of the CT grid. When these ray average concentrations were used to reconstruct the spatial distribution of acetone concentrations, the program produced the image illustrated in Figure 4. Though clearly much more comparable to the FID map (Figure 2) than the reconstruction from the measured path averages (Figure 3), some disagreement at the level of individual pixels remains. However, the low value of sigma, 0.002, reflects the fact that almost all ray averages of the reconstructed picture match those of the kriged data to better than 0.6 percent.

DISCUSSION

Figures 2 and 3 show similarity between the CT reconstruction and the concentration map generated from the FID array measurements. The CT reconstruction correctly located the position of the source and reproduced the steep concentration profile surrounding it. However, many notable differences also appear; the CT image shows a trailing plume while the FID image has none, and the peak height at the source is almost double in the CT picture. These differences raise the issues of whether the FID image or the CT image show the "true" picture and what factors may have contributed to the discrepancy.

There are substantial limitations in both the CT and the FID projection data as obtained in this experiment. For example, to ensure that the concentration pattern remains absolutely stable, the CT data should be collected so that the instrument would not change the airflow. At some, but not all positions, the detector optics were in the airflow upstream of the acetone source. Modifications to the airflow in the measurement plane owing to the withdrawal of air through the FID sampling array probably had little effect, because a fairly low flow rate was used for sampling through each tube (5 cc/sec). Velocity changes at the sample inlet should drop off quickly to below background levels within a few mm of the FID sample tube inlet.

Positioning the FID sample array represents another limitation. Ideally, the point samples would be in a plane coincident with the CT scan at the same height as the source. Of course, it is impossible to have a sampling point coincident with the source. In our experiments, the IR beams were approximately 5 cm (2 inches) in diameter. To avoid blocking the beams with the FID sampling tubes, the tubes were positioned so their tips grazed the bottom edge of the beams. This placed the plane of the FID sampling tubes about 2 cm below the plane of the beam centerlines, and about 5 cm below the center of the source.

To explore the influence of the small vertical separation (2 cm) between the FID and the FTIR sampling plane, the authors modeled transport near the point source based on isotropic eddy diffusion in a uniform flow.[26] Under these conditions the concentration field around the source can be described by the equation:[27]

$$C_r = \frac{\dot{m}}{4\pi K r} e^{\frac{u(x-r)}{2K}}$$

where

C_r = concentration at r (mg/m^3)

$r = \sqrt{x^2 + y^2 + z^2}$ distance from point source (m)

$\dot{m}$ = mass generation rate (mg/min)

u = air velocity (m/min) (aligned with x axis)

K = eddy diffusivity (m^2/min)

x = distance in x direction (m).

Employing an approach similar to Roach,[28] the authors estimated the effective diffusivity by calculating K from the above equation using nine kriged FID concentration values located within a 40-cm radius of the source. All calculations assumed a source emission rate of 1 g/min (based on a saturated source gas) and an air velocity of 6 m/min (based on exhaust air concentration readings). Combining the estimates yielded an average value for the effective diffusivity of 1.28 m^2/min. Using this average value of K, the calculated concentration for the FID peak 5 cm below the source was 466 ppm, and for the FTIR peak 3 cm below the source was 813 ppm. These calculated values agree quite well with the observed peaks for the FID array (472 ppm) and the CT reconstruction (880 ppm). Thus the placement of the FTIR beam measurements in a plane slightly closer to the source compared to the FID array probably accounts for the difference in the peak concentration.

The results from the synthetic CT reconstruction of the FID data (Figure 4) appear to match the original FID image closely (Figure 2) both in terms of the peak height and peak shape, with some overall broadening of the peak and lowering of the peak concentration. This strongly suggests that the differences between Figure 2 and Figure 3 are not due to some inadequacy in the algorithm, but rather to inconsistencies in the input data. This also is indicated by the much higher values of sigma in the CT image (Figure 3) compared to the CT image of the FID data (Figure 4).

Three factors limit the CT reconstruction accuracy: noise, the nonuniqueness of the CT solution, and the spatial sampling frequency. Noise in this sense represents time and space variability in the concentration pattern due to a variety of factors; changes in the airflow pattern and vortex shedding from the instrument in the airflow, positioning errors, and measurement errors all contribute to variability in the path-averaged concentrations. Position errors introduced by limitations in the mechanical system were generally small, typically less than 3 mm (1/8"), and would produce relative errors in position on the order of a fraction of a percent.

The authors attempted to reduce the effects of temporal fluctuations in concentration at fixed positions in space by averaging each ray over time (typical SD of ray averages ~ 30%). They compared the timescale of the averaging to estimates of the frequency of vortex shedding from objects (cylinders) in the airflow. For an air velocity of 10 cm/sec and cylinders of 1 to 50 cm in diameter (the range of obstacle sizes in our experiment), the frequency of vortex shedding was estimated to be between 0.04 and 1.5 Hz.[29] This indicates that the longest timescales are on the order of 25 sec, far shorter than the 5 min averaging times for the rays. Perhaps a more important source of error in the projection data may have been changes in the air flow and plume dispersion pattern as the instrument was rotated to different angles, rather than eddy shedding.

The effect of changing the dispersion pattern during the experiment is to present the reconstruction algorithm with an inherently inconsistent set of data; this is equivalent to trying to reconstruct projections sampled from several different spatial distributions of contaminant. Such data cannot necessarily be assembled to create an image that simultaneously satisfies all ray averages. This lack of consistency manifests itself in the inability to converge further after a certain number of iterations, despite relatively poor agreement between

calculated and measured ray average concentrations. The high value of sigma for Figure 3 is an indication that a single spatial distribution of acetone satisfying the measured set of path average concentrations probably did not exist. In contrast, the reconstruction of the synthetic projections derived from the kriged FID data produced a low sigma value that constantly decreased with an increasing number of iterations, reflecting the fact that there was at least one distribution that matched the given path-average projection data.

Spatial resolution limits the FID sampling data, perhaps to a more severe degree than the RS-FTIR. If each FID sample point only reflects concentrations within the immediate few cm of surrounding space, relatively small horizontal shifts in the location of the plume could cause dramatic changes in the concentrations measured by the FID. The RS-FTIR, however, would still capture the plume because of the much larger sampling path. Thus, spatial-temporal variability in the plume location within the measurement plane is a possible explanation for differences between the measurements.

It is important to point out that if changes in the dispersion pattern did occur as a result of different instrument positions at different times during the experiment, both the kriged map and the CT reconstruction would give an inaccurate picture. Like the CT data, the kriged data was sampled systematically from different instrument locations and at different times, and could be due to different underlying spatial distributions. Kriging this data would tend to add sampled points from the different spatial distributions together to produce a map, while CT reconstruction would tend to average the distributions. The two techniques will produce different concentration maps from the data, but one map is not necessarily more correct than the other.

The second important limit on reconstructing the actual concentration distribution stems from the fact that the system of equations was underdetermined. In theory, complete determination of the image would be possible only if the number of rays matched the number of pixels and the rays were distributed appropriately. Since the reconstruction matrix size is approximately the square of the number of rays per projection (ignoring the edges), this implies that the number of projection angles should at least equal the number of rays per projection. In iterative computed tomography, if the number of projections in the input data is small, the reconstruction tends to predict concentration peaks that are lower than the true maxima.[16]

The limited number of projections (four rather than the necessary minimum of nine) in the experiment leads to the fact that even perfectly consistent data, namely those ray averages calculated directly from the kriged FID data, did not lead to a perfect reconstruction. When comparing Figures 2 and 4, we see that the reconstructed image (Figure 4) has peaks that are broader and lower than the input data, despite convergence to a low sigma value. Thus, unless the conditions for uniqueness of the solution to the equations represented by the ray averages are met, a low sigma value does not guarantee that a unique concentration distribution has been determined. A low sigma value merely indicates convergence to one of many possible solutions.

Underdetermination does not provide a likely explanation for the discrepancy between Figures 2 and 3. In contrast to expectation the peak in the FTIR reconstruction (Figure 3) is higher and narrower than the FID data would suggest. Also, sigma is relatively high for Figure 3, indicating that no single distribution matched even the limited ray data that was provided. This is the opposite of the problem of underdetermination, where there are too many solutions so the program fails to converge to the true one.

A third limit on CT reconstruction is the spatial sampling frequency, referring to the number of rays per unit of projection length (i.e., the sample frequency f in rays/m). Intuitively, one recognizes the importance of the sampling frequency when trying to capture a steep concentration gradient. For example, to measure a situation where the concentration changes from near background to a peak over a distance of d = 0.3 m (1 ft), one must sample at intervals smaller than d. Sampling over much larger intervals will result in a poor reconstruction of the actual concentration, either by missing the peak or underestimating the gradients. In general, to satisfy the Nyquist criterion one needs $f * d \geq 2$, where d is the smallest dimension to be resolved in the physical system. The CT results presented here had a sampling frequency of 3 rays/m, which despite the correspondingly limited spatial resolution appeared to reasonably capture a large concentration gradient and correctly identify the peak location. The important point remains, however, that the sampling frequency is not simply an arbitrary quantity dictated by the desired image resolution but one that ultimately depends on the physical distribution under study.

One motivation for choosing a remote optical sensing system is its nonobtrusive nature. However, the system tested here could not fully realize this goal because of limitations imposed by the sizes of the room, the instrument, and the test apparatus.

A second motivation is the potential for rapid sampling. Although the RS-FTIR gathers data very quickly (up to two readings per second), rapid scanning could not be achieved due to limitations in the positioning system. In fact, the ray path sampling procedure was quite slow, comparable in speed to the conventional FID sampling technique. Better RS-FTIR sampling technology, such as a scanning system employing moving mirrors, multiple mirrors, or multiple sources and detectors as suggested by Todd and Leith,[14] could realize more fully the potential for unobtrusive and rapid sampling.

This article has demonstrated the application of CT to an important class of problems: in situ measurements of gaseous dispersion. Whether dedicated to outdoor readings, workplace situations, or to indoor air measurements, the problems outlined above must be addressed. The issues of indeterminacy and spatial resolution are essentially technical limitations, in that both can be solved by gathering more data. These factors may have contributed to the discrepancies in our reconstruction data. However, the effects of sample point location and temporal variability remain a likely explanation for the disagreement between the FID point data and the CT image, as suggested by the high value of sigma

for that reconstruction. Interestingly, there are two ways to address temporal variability in the projection data; one is to quickly sample all rays simultaneously obtaining a snapshot view. The other approach is to measure time-averaged concentrations over long periods. The authors attempted the latter method with only limited success, suggesting that more rapid sampling may be necessary.

In summary, this work demonstrates for the first time the feasibility of CT reconstructions of pollutant concentrations in a real room setting. Good qualitative agreement between the reconstruction and point sample data was obtained. The limitations encountered due to the temporal resolution, size, and geometry of the experimental apparatus are clearly surmountable with better instrumentation.

ACKNOWLEDGEMENTS

The authors would like to thank Jyun-De Wu, John Potter, Stuart Foster, and Dr. Bill Herget for their expert technical assistance, and Nicolet Instruments for technical support.

REFERENCES

1. **Bauman F., A.J. Gadgil, R. Kammerud, E. Altmayer, and M.W. Nansteel:** Convective heat transfer in buildings: Recent research results. *ASHRAE Trans. 89(1A)*:215–232 (1983).
2. **Yost M.G. and R.C. Spear:** Measuring Indoor Air Flow Patterns Using a Sonic Vector Anemometer. *Am. Ind. Hyg. Assoc. J. 53*:677–680 (1992).
3. **Murakami S., S. Kato, and Y. Suyama:** Numerical study on diffusion field as affected by arrangement of supply and exhaust openings in conventional flow type clean room. *ASHRAE Trans.* 1992. [In press]
4. **American Society for Testing and Materials:** Standard test method for determining air leakage rate by tracer dilution. (ASTM E 741-83) In *Annual Book of ASTM Standards.* Philadelphia: American Society for Testing and Materials, 1983. Sec. 4, Vol. 04.07.
5. **W.J. Fisk, R.J. Prill, and O. Seppanen:** *Commercial building ventilation measurements using tracer gases.* (LBL report #LBL-25612) Berkeley, CA: Lawrence Berkeley Laboratory, 1988.
6. **Grant W.B. and R. T. Menzies:** A survey of laser and selected optical systems for remote measurement of pollutant gas concentrations. *J. Air Pollution Cont. Assoc. 33*:187–194 (1983).
7. **Levine, S.P., L.S. Ying, C. Strang, and X. Hong-Kui:** Advantages and disadvantages in the use of Fourier transform infrared (FTIR) and Filter IR (FIR) spectrometers for monitoring airborne gases and vapors of industrial hygiene concern. *Appl. Ind. Hyg. 4(7)*:180–187 (1989).
8. **Faris, G.W. and R.L. Byer:** Quantitative optical tomographic imaging of a supersonic jet. *Optics Lett. 11*:413–415 (1986).
9. **Faris, G.W. and R. L. Byer:** Quantitative three-dimensional optical tomographic imaging of supersonic flows. *Science 238*:1700–1702 (1987).
10. **Liu, T.C., W. Merzkirch, and K. Oberste-Lehn:** Optical tomography applied to speckle photographic measurement of asymmetric flows with variable density. *Exp. Fluids. 7*:157–163 (1989).
11. **Faris, G.W. and R.L. Byer:** Beam deflection optical tomography of a flame. *Optics Lett. 12*:155–157 (1987).
12. **D.C. Wolfe:** "On the Application of Optical Computed Tomography to Remote Air Pollution Measurements." Ph.D. diss., Stanford University, Palo Alto, CA (1980).
13. **Wolfe, D.C. and R.L. Byer:** Model studies of laser absorption computed tomography. *Appl. Optics 21*:1165–1178 (1982).
14. **Todd, L. and D. Leith:** Remote sensing and computed tomography in industrial hygiene. *Am. Ind. Hyg. Assoc. J. 51*:224–233 (1990).
15. **Todd, L.A.:** Optical Remote Sensing/Computed Tomography Systems for Workplace Exposure Assessments. In *Proceedings on Optical Remote Sensing Applications to Environmental and Industrial Safety Problems. Air Waste Manage. Assoc. SP81*:356–360 (1992).
16. **Todd, L.A.:** Optical Remote Sensing/Computed Tomography Beam Geometries for Monitoring Workplace Gases and Vapors. In *Proceedings on Optical Remote Sensing Applications to Environmental and Industrial Safety Problems. Air Waste Manage. Assoc. SP81*:390–393 (1992).
17. **Yost, M.G., H.K. Xiao, R.C. Spear and S.P. Levine:** Comparative Testing of a FTIR Remote Optical Sensor with Area Samplers in a Controlled Ventilation Chamber. *Am. Ind. Hyg. Assoc. J. 53*:611–616 (1992).
18. **Xiao, H.K., S.P. Levine, W.F. Herget, J.B. D'Arcy, R.C. Spear, T. Prichett:** A transportable remote sensing infrared air monitoring system. *Am. Ind Hyg. Assoc. J. 52*:4375–5381 (1991).
19. **Ying, L.S. and S.P. Levine:** Fourier transform infrared least-squares methods for the quantitative analysis of multicomponent mixtures of airborne vapors of industrial hygiene. *Concern. Anal. Chem. 61*:677–683 (1989).
20. **Jones, T.A., D.E. Hamilton and C.R. Johnson:** *Contouring Geologic Surfaces with the Computer.* New York: Van Nostrand Reinhold, 1986.
21. **Kak, A.C. and M. Slaney:** *Principles of Computerized Tomographic Imaging.* New York: IEEE Press, 1988.
22. **Hertz, H.M.:** Experimental Determination of 2-D Flame Temperature Fields by Interferometric Tomography. *Optics Comm. 54(3)*:131–136 (1985).
23. **Brooks R.A. and G. Di Chiro:** Theory of Image Reconstruction in Computed Tomography. *Radiology 117*:561–572 (1975).
24. **Peterson, J.E.:** "The Application of Algebraic Reconstruction Techniques to Geophysical Problems." Ph.D. diss., Dept of Geophysics, University of California, Berkeley, CA, 1986.
25. **Fraser, M.:** Summer Study at Indoor Environment Program. [Unpublished results] 1 Cyclotron Rd. Bld 90, Lawrence Berkeley Laboratory, Berkeley, CA, 1989.
26. **Roberts, O.F.B.:** The Theoretical Scattering of Smoke in a Turbulent Atmosphere. *Proc. Royal Soc. Series A 104*:640–654 (1923).
27. **Seinfeld, J.:** *Atmospheric Chemistry and Physics of Air Pollution.* New York: John Wiley, 1986.
28. **Roach, S.A.:** On the Role of Turbulent Diffusion in Ventilation. *Ann. Occ. Hyg. 24(1)*:105–132 (1981).
29. **Schlichting, H.:** Boundary Layer Theory, 7th. ed. New York: McGraw-Hill, 1979.